

COLORECTAL CANCER TUMOR GRADE SEGMENTATION IN DIGITAL HISTOPATHOLOGY IMAGES: FROM GIGA TO MINI CHALLENGE

*Alper Bahcekapili*¹ *Duygu Arslan*¹ *Umut Ozdemir*¹ *Berkay Ozkirli*¹
Emre Akbas^{1,2} *Ahmet Acar*¹ *Gozde B. Akar*¹ *Bingdou He*³
*Shuoyu Xu*³ *Umit Mert Caglar*¹ *Alptekin Temizel*¹ *Guillaume Picaud*⁴
*Marc Chaumont*⁴ *Gérard Subsol*⁴ *Luc Téot*⁶ *Fahad Alsharekh*⁷
*Shahad Alghannam*⁷ *Hexiang Mao*⁸ *Wenhua Zhang*⁹

¹Middle East Technical University, Ankara 06800, Türkiye ²Helmholtz Munich, Germany

³Bio-totem Pte Ltd, Suzhou, P.R. China ⁴LIRMM, équipe ICAR, Univ. Montpellier, CNRS, France

⁵Univ. Nîmes, Place Gabriel Péri, France ⁶Cicat-Occitanie, Montpellier, France

⁷Thiqah Business Services Riyadh, Saudi Arabia ⁹Shanghai University Shanghai 200444, China

⁸Nanjing Tech University, Nanjing, Jiangsu 211816, China

ABSTRACT

Colorectal cancer (CRC) is the third most diagnosed cancer and the second leading cause of cancer-related death worldwide. Accurate histopathological grading of CRC is essential for prognosis and treatment planning but remains a subjective process prone to observer variability and limited by global shortages of trained pathologists. To promote automated and standardized solutions, we organized the ICIP Grand Challenge on Colorectal Cancer Tumor Grading and Segmentation using the publicly available METU CCTGS dataset. The dataset comprises 103 whole-slide images with expert pixel-level annotations for five tissue classes. Participants submitted segmentation masks via Codalab, evaluated using metrics such as macro F-score and mIoU. Among 39 participating teams, six outperformed the Swin Transformer baseline (62.92 F-score). This paper presents an overview of the challenge, dataset, and the top-performing methods.

Index Terms— Digital histopathology, colorectal cancer, tumor grade segmentation.

1. INTRODUCTION

Colorectal cancer (CRC) represents the third most frequently diagnosed malignancy globally, accounting for over 1.8 million new cases annually [1], and stands as the second leading cause of cancer-related mortality worldwide [2]. Epidemiological projections anticipate a significant increase in

incidence, with an estimated 3.2 million new CRC cases expected by 2043 [3]. The disease is characterized by considerable pathophysiological heterogeneity, encompassing multiple histological subtypes, each with distinct prognostic and therapeutic implications [4]. Histopathological evaluation of tissue specimens obtained via colonoscopy or surgical resection remains the gold standard for diagnosis. Distinguishing benign and malignant neoplasms and accurately determining tumor grade are essential components of routine pathological assessment. Tumor grade holds well-established prognostic significance, with poor differentiation strongly associated with adverse clinical outcomes, and plays a critical role in guiding therapeutic decision-making [5–7].

Despite its diagnostic relevance, histopathological grading is inherently subjective and prone to both inter- and intra-observer variability, often influenced by the level of expertise and experience of individual pathologists [8,9]. This variability is further exacerbated by significant global disparities in the availability of trained pathology professionals, with some regions reporting fewer than three pathologists per million inhabitants [10]. These challenges highlight the urgent need for scalable, automated solutions to support and standardize diagnostic workflows.

To address this need, we organized the ICIP Grand Challenge on Colorectal Cancer Tumor Grading and Segmentation¹. The challenge utilized the METU CCTGS dataset [11], a recent, publicly available dataset. It consists of 103 whole-slide histopathology images (WSIs) from 103 patients, acquired at varying magnifications. Expert pathologists provided pixelwise annotations for five classes: tumor grades 1–3, normal mucosa, and others. The dataset includes both original high-resolution SVS files and their downsized ver-

¹This work has been supported by Middle East Technical University Scientific Research Projects Coordination Unit under grant numbers ADEP-704-2024-11486 and ADEP-312-2024-11455. The numerical calculations reported in this paper were performed at TUBITAK ULAKBIM, High Performance and Grid Computing Center (TRUBA). Dr. Akbas gratefully acknowledges the support of TUBITAK 2219.

⁴Thanks to the ANRT and Cicat-Occitanie for funding.

¹<https://sites.google.com/view/cctgs-challenge>

sions. Further details on the dataset can be found in [11].

We partitioned the dataset into training (70%), validation (15%), and testing (15%) subsets using stratified random sampling to maintain class distribution balance at the pixel level. Both SVS files and downsized images for all three splits were provided to participants. Only the labels for the training and validation sets were shared. Participants submitted predicted segmentation masks to an evaluation server on Codalab², which scored the submissions using the hidden test labels and returned performance metrics including F-score, precision, recall, and mean Intersection-over-Union (mIoU).

A total of 39 teams participated in the challenge. To ensure reproducibility, participants were required to submit Docker files along with their code. We verified that the reported results could be reproduced using these Docker environments and reviewed the submitted code to ensure that no inappropriate machine learning practices were used. Submissions were ranked based on the macro F-score across the five classes. From those who submitted the docker files, only six teams outperformed the 62.92 macro F-score baseline obtained by Swin Transformer [11]. In the following sections, we summarize these top six methods and evaluate the results.

2. METHODS

This section summarizes the top six methods, in the order of decreasing performance. The methods range from novel combinations of different models to careful fine-tuning of already existing models. Notably, only the top two teams utilized the full-resolution whole-slide images (i.e., large SVS files), and their performance was significantly better than the rest. Additionally, the top three teams employed ensembles of several models through voting. Before this challenge, the best performance on the METU CCTGS dataset was 62.92 macro F-score; at the end of the challenge, the best score is now 70.2.

2.1. VAN+UperNet³

Model Architecture. The method uses the UperNet architecture [12] with a Visual Attention Network (VAN) [13] backbone. Training was initialized using ImageNet-pretrained weights. An auxiliary Fully Convolutional Network head [14] was added, and both heads contributed to the total loss via separate loss calculations.

Training: Three models were trained via three-fold cross-validation. During training 512x512 crops were taken from the whole slide images using a active cropping method to sample regions based on label distributions. Each WSI was divided into a dense grid of candidate regions, with each patch scored according to the class-weighted sum of its pixels, allowing the system to sample patches proportionally to their semantic richness. This selection provides better coverage of rare classes and as a result it's particularly well-suited for histopathology, where foreground areas are sparse relative to

background. Each resulting crop was then normalized and augmentations such as random rotations within the range of -45 to +45, random 90 counterclockwise rotations (1 to 3 times), symmetric flipping, color perturbations in the HSV space, and random scaling within a factor range of [1.0, 1.5] were applied.

A smaller learning rate was applied to the encoder than the decoder, 0.0001 and 0.001, respectively. The loss function used combines Dice loss and cross-entropy loss, incorporating both label smoothing and maximal restriction strategies in the loss calculation. The "background" class was excluded from loss computation. The Adam optimizer with a cosine warm-up schedule was used, with a batch size of 12, for a total of 40 epochs. The best-performing model was selected based on the highest average DICE score on the validation set.

Inference: For inference, each WSI was split into 1024x1024 overlapping patches (50% overlap). Patches were segmented independently by three models; their outputs were multiplied with a Gaussian kernel to emphasize central regions. The resulting class probability maps were accumulated and normalized to produce a unified per-pixel probability tensor. Final heatmaps were obtained by averaging predictions from all three models, and the final segmentation masks were produced by assigning each pixel to the class with the highest predicted score. These masks were then resized to the test set dimensions using nearest-neighbor interpolation, ensuring that discrete class labels were preserved. Finally, postprocessing was performed on the resized mask: for each class of interest, external contours were extracted and re-drawn to fill small holes and correct fragmented shapes.

2.2. DPT+MaxViT⁴

Model Architecture: A set of multiple Dense Prediction Transformer (DPT) models [15] and Multi-Axis Vision Transformer (MaxViT) [16] encoders of varying sizes are trained to ensure strong generalization to real test data. Models in this set used different input scalings of data, different patch sizes, strides and loss functions.

Training: Crops of size 2048x2048 were taken out of whole slide images and then downsampled. Adaptive augmentation policy optimization with LLM feedback [17] was used in training, enabling the adaption of various models and configurations to the same dataset and task. It was shown that optimizing augmentation policy adaptively improved the overall training performance and robustness of the trained models.

Inference: For model output handling, nearest-neighbor interpolation was used when downscaling segmentation masks to preserve class labels, while bilinear and area interpolation were also applied depending on the target. Area interpolation was particularly useful for per-pixel probability matrices, commonly applied in topographical analysis and well-suited for histopathology WSIs due to its ability to maintain regional structures [18].

²<https://codalab.lisn.upsaclay.fr/competitions/22064>

³Contributed by He Bingdou and Xu Shuoyu.

⁴Contributed by Ümit Mert Çağlar and Alptekin Temizel.

Initially, a hard-voting ensemble was applied by majority voting over the predicted masks. This straightforward approach improved the top-performing model’s mean F1 score from 67.11 to 69.07. To further improve segmentation performance, a soft voting ensemble strategy was implemented. Instead of voting on the discrete segmentation masks, the class-wise probability distributions output by each model were aggregated. For each pixel location, the predicted top-N probabilities across a selected best-performing M models were summed, and a soft class-specific bias vector was applied. This bias vector favored tumor-related classes and reduced the influence of the background predictions. Final masks were obtained by assigning each pixel to the class with the highest probability in the aggregated tensor. This Top-N Soft Biased Voting method achieved another boost, raising the mean F1 score to 69.73.

To refine the output of the ensemble segmentation masks and further reduce prediction noise, a three-stage postprocessing pipeline was applied. This final refinement step helped eliminate minor artifacts and boosted the final mean F1 score to 69.84 on the test set. A Gaussian filter was applied to the ensembled prediction probability maps to spatially smooth the probabilities before thresholding. This helped integrate contextual information around each pixel, mitigating sharp and isolated errors often observed at tumor boundaries. The binarized segmentation masks were refined using morphological closing operations (dilation followed by erosion) to fill small holes and close narrow gaps, improving the shape integrity of predicted tumor regions and aligning better with histopathological patterns. Small spurious components were removed by discarding connected regions with area below a dataset-specific threshold ϵ , as these were typically noise or false positives introduced by edge uncertainty.

2.3. HardNet+Lawin⁵

Model Architecture HardNet-DFUS [19] is a segmentation model that combines a lightweight convolutional encoder, HardNet [20], with a transformer-based decoder, Lawin [21]. Feature maps are extracted at four levels of the encoder, enabling the decoder to exploit multi-scale representations. The final three feature maps are passed through MLP layers, concatenated, and then fed into the Lawin modules [21]. The first feature map is processed through an MLP and injected at the end of the decoder, helping preserve spatial information. The overall model architecture is illustrated in Figure 1.

Training: Firstly, the HardNet encoder was retrained for tissue patch classification using the NCT-CRC-HE-100K-NONORM dataset [22]. A classification head was appended to the encoder and trained by cross-entropy loss. Although the pretraining dataset has known biases [23], the pretrained weights sped up convergence and boosted early validation

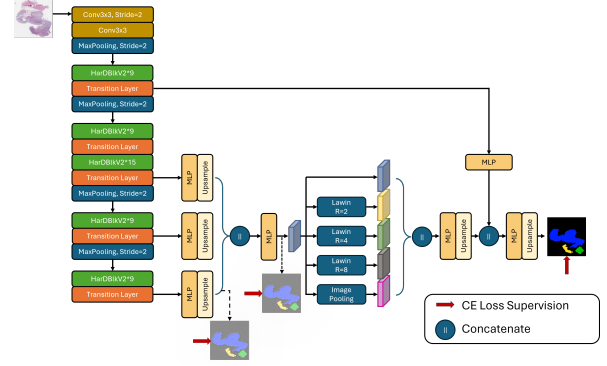


Fig. 1. Model architecture for the “HardNet+Lawin” method.

performance. Three unfreezing schedules, fully frozen encoder, warm up, and progressive unfreezing, were compared against one and another and it was found that, the warm-up strategy provided the most consistent validation improvements.

Weights learned from the pretraining step were used to initialize the encoder part of the HardNet-DFUS model for the segmentation task. Cross-entropy loss function and the AdamW optimizer with an initial learning rate of $1e-4$ (scheduled via cosine annealing) and an Exponential Moving Average of the weights were employed during training. Downsampled version of the CCTGS dataset was used. To mitigate catastrophic forgetting, a warm-up phase of two epochs at the beginning of training was included [24]. Images were resized to 1536×1536 pixels and batch size of two was selected due to memory limitations. A standard data augmentation pipeline, combining geometric transformations including flipping, shifting, scaling and rotation and color transformations including color jittering, coarse dropout and Gaussian Noise was applied. The proposed training strategy was applied using 5-fold cross-validation, with the mean F1-score as the validation metric.

Inference: To address performance variability across folds, an ensembling strategy by selecting the top three models, applying test-time augmentation (TTA) independently to each, and aggregating their predictions through majority voting was adapted. The final predictions were post-processed using hole filling.

2.4. Segmenter-L⁶

This method basically fine-tunes a pre-trained, off-the-shelf Segmenter-L with ViT backbone model from MMSegmentation [25]. The model was pre-trained on the ADE20K dataset.

2.5. SegFormer-B1⁷

This method basically fine-tunes a pre-trained, off-the-shelf SegFormer-B1 model from the MMSegmentation repository [25]. The model was pre-trained on the Cityscapes dataset.

⁵Contributed by Guillaume Picaud, Marc Chaumont, Gérard Subsol and Luc Téot.

⁶Contributed by Fahad Alsharekh.

⁷Contributed by Shahad Alghannam.

2.6. PathVTA⁸

Model Architecture: It consists of three key components: (1) the UNI [26] foundation model serving as the feature extractor, (2) a ViT Adapter [27] module that yields a multi-scale feature pyramid, and (3) a UNet-style decoder that restores spatial resolutions and predicts the segmentation mask. The UNI backbone is frozen, and only the adapter and decoder are trained.

Training: PathVTA was trained on the down-scaled dataset. To improve data diversity, augmentation techniques such as random cropping, rotations and flips as well as color jittering, gaussian blur and photometric distortion were employed. Training was performed for 5,000 iterations using cross-entropy loss. Adam optimizer with an initial learning rate of 0.0002 was used to train the network.

Inference: To handle high-resolution inputs, a sliding window inference strategy with a window size of (224, 224) and a stride of (112, 112) employed. For each extracted patch, the model outputs logits, which are converted to class probabilities via softmax. For overlapping regions, predicted probabilities are accumulated. Then, a second softmax is applied to normalize the aggregated probability map. Finally, the segmentation prediction is obtained by performing the argmax over the normalized map.

3. RESULTS

Performances of the six contributed methods can be seen in Table 1. Although the dataset included large whole-slide images (WSIs), only two teams used them—likely because handling and processing such high-resolution files is technically challenging. However, we see a clear benefit of using WSIs on test metrics. The top two teams both utilized WSI and they are both at least 3 points above the third team. Utilizing features extracted from the original high-resolution whole slide images (WSIs), as opposed to their downsampled counterparts, allows models to capture richer morphological details, thereby enabling more accurate and fine-grained analysis. Another trend we see is that the methods using voting mechanism tended to perform better than others. This may be because ensembling combines the strengths of multiple models, leading to more robust and accurate predictions than single-model approaches.

Representative qualitative results for tumor grade segmentation generated by the top six methods are shown in Figure 2, highlighting their comparative performance across different histopathological cases. **VAN+UperNet** demonstrates high precision in identifying semantic class boundaries, even for non-convex and non-compact objects. It successfully detects normal mucosa with minimal omission. Although it shows some confusion between Grade 1 and Grade 2 tumors, it performs well in distinguishing Grade 3 tumors, rarely misclassifying them as Grade 2 and generally separating them

clearly from other tumor types. In terms of minimizing confusion between Grade 1 and Grade 2, it ranks among the top-performing methods after SegFormer-B1. Compared to VAN+UperNet’s results, **DPT+MaxViT** tends to label larger areas as Grade 3 in Grade 3-positive images. It effectively segments normal mucosa, even when boundaries are non-convex. However, it struggles with distinguishing between Grade 1 and Grade 2 tumors. Like VAN+UperNet, it often labels ambiguous “others” regions as Grade 3 in Grade 3-positive images. **HardNet+Lawin** tends to over-connect boundaries when segmenting non-convex normal mucosa regions. It shares similar issues with other methods in confusing Grade 2 and Grade 3 tumors, but demonstrates a lower tendency to detect Grade 3 regions in images that contain them, often missing these tumors.

In summary, VAN+UperNet appears to offer the most balanced performance in preserving class boundaries and minimizing confusion, particularly for complex tumor morphologies. SegFormer-B1 excels in grade separation but is limited by fragmented predictions. Segmenter-L and DPT+MaxViT exhibit strong detection for certain classes but suffer from over-segmentation and grade confusion. HardNet+Lawin underperforms in high-grade detection, while PathVTA show extensive misclassifications and it is particularly prone to inter-grade confusion. Overall, while each method has strengths, challenges remain particularly in resolving boundary-level ambiguities and differentiating intermediate-grade tumors. These observations reinforce the need for robust spatial modeling and grade-aware architectures in semantic segmentation for tumor analysis.

The consistency and style of training annotations could be studied. By visualizing training annotations, we distinguished two annotation methods: one produces masks with smoothed boundaries, while the other yields masks with highly detailed edges. This discrepancy introduces learning challenges, as alternating between annotation domains may lead to undesired biases. It also complicates model evaluation, since there is no clear guidance on which annotation domain should be prioritized.

4. CONCLUSION

The ICIP Grand Challenge on Colorectal Cancer Tumor Grading and Segmentation aimed to address the pressing need for accurate models for tumor grading and segmentation in histopathology by benchmarking algorithms on a realistic dataset. The challenge attracted broad participation, with 39 teams developing segmentation models for complex multi-class tissue grading and segmentation under limited supervision. The top-performing methods demonstrated the potential of advanced deep learning models, particularly transformer-based architectures, for handling high-resolution whole-slide images with dense pixelwise annotations. Model ensembling also stood out as an important technique for improved accuracy.

⁸Contributed by Hexiang Mao and Wenhua Zhang.

Table 1. Performances of top six methods and the baseline.

Method	Notes	mFscore	mIoU	mPrecision	mRecall
VAN+UperNet	WSI & ensemble	70.2	56.5	67.2	74.4
DPT+MaxViT	WSI & ensemble	69.8	55.8	68.6	71.7
HardNet+Lawin	ensemble	66.7	52.8	63.0	72.4
Segmenter-L		65.2	51.3	63.7	67.5
Segformer-B1		65.1	50.7	61.2	70.6
PathVTA		64.2	50.2	63.3	65.7
SwinTransformer [11]	baseline	62.9	-	60.9	69.6

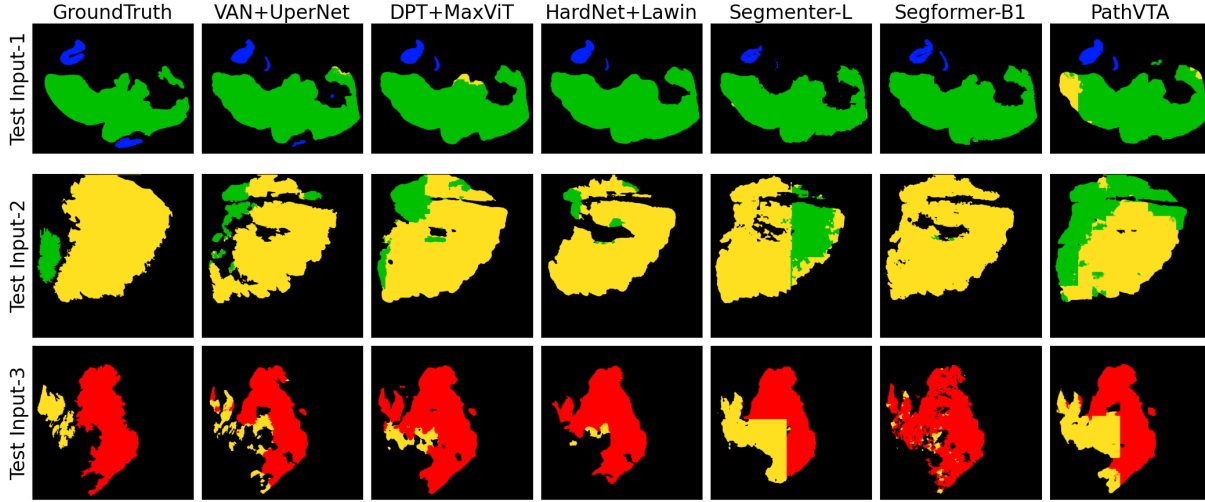


Fig. 2. Qualitative experimental results for Top-6 best performing methods for 3 input test images. (Color codes for classes: Blue:Normal mucosa, Green:Grade-1, Yellow:Grade-2, Red: Grade-3, Black:Others)

While the leading approaches showed promise, the overall performance margins indicate that histopathology tumor grading and segmentation remains a difficult task, especially in discriminating between tumor grades. These findings highlight opportunities for future research, including more effective use of multi-scale information and better data efficiency in training. The METU CCTGS dataset and the evaluation infrastructure remain publicly available, encouraging continued progress in this critical area of medical image analysis.

5. REFERENCES

- [1] Hyuna Sung, Jacques Ferlay, Rebecca L Siegel, Mathieu Laversanne, Isabelle Soerjomataram, Ahmedin Jemal, and Freddie Bray, “Global cancer statistics 2020: Globocan estimates of incidence and mortality worldwide for 36 cancers in 185 countries,” *CA: a cancer journal for clinicians*, vol. 71, no. 3, pp. 209–249, 2021.
- [2] Rebecca L Siegel, Kimberly D Miller, Ann Goding Sauer, Stacey A Fedewa, Lynn F Butterly, Joseph C Anderson, Andrea Cercek, Robert A Smith, and Ahmedin Jemal, “Colorectal cancer statistics, 2020,” *CA: a cancer journal for clinicians*, vol. 70, no. 3, pp. 145–164, 2020.
- [3] Yue Xi and Pengfei Xu, “Global colorectal cancer burden in 2020 and projections to 2040,” *Translational oncology*, vol. 14, no. 10, pp. 101174, 2021.
- [4] Justin Guinney, Rodrigo Dienstmann, Xin Wang, Aurélien De Reynies, Andreas Schlicker, Charlotte Soneson, Laetitia Marisa, Paul Roepman, Gift Nyamundanda, Paolo Angelino, et al., “The consensus molecular subtypes of colorectal cancer,” *Nature medicine*, vol. 21, no. 11, pp. 1350–1356, 2015.
- [5] Yong Beom Cho, Ho-Kyung Chun, Hae Ran Yun, Hee Cheol Kim, Seong Hyeon Yun, and Woo Yong Lee, “Histological grade predicts survival time associated with recurrence after resection for colorectal cancer,” *Hepato-gastroenterology*, vol. 56, no. 94-95, pp. 1335–1340, 2009.
- [6] IP Chandler and RS Houlston, “Interobserver agreement in grading of colorectal cancers—findings from a nationwide web-based survey of histopathologists,” *Histopathology*, vol. 52, no. 4, pp. 494–499, 2008.

- [7] Mahul B Amin, Frederick L Greene, Stephen B Edge, Carolyn C Compton, Jeffrey E Gershenwald, Robert K Brookland, Laura Meyer, Donna M Gress, David R Byrd, and David P Winchester, “The eighth edition ajcc cancer staging manual: continuing to build a bridge from a population-based to a more “personalized” approach to cancer staging,” *CA: a cancer journal for clinicians*, vol. 67, no. 2, pp. 93–99, 2017.
- [8] Christophe Klein, Qinghe Zeng, Floriane Arbaretaz, Estelle Devèvre, Julien Calderaro, Nicolas Lomenie, and Maria Chiara Maiuri, “Artificial intelligence for solid tumour diagnosis in digital pathology,” *British Journal of Pharmacology*, vol. 178, no. 21, pp. 4291–4315, 2021.
- [9] GD Thomas, MF Dixon, NC Smeeton, and NS Williams, “Observer variation in the histological grading of rectal carcinoma,” *Journal of Clinical pathology*, vol. 36, no. 4, pp. 385–391, 1983.
- [10] A Bychkov and M Schubert, “Constant demand, patchy supply,” *Pathologist*, vol. 88, no. 88, pp. 18–27, 2023.
- [11] Duygu Arslan, Sina Sehlaver, Erce Guder, M. Arda Temena, Alper Bahcekapili, Umut Ozdemir, Duriye Turkay, Gunes Guner, Servet Guresci, Cenk Sokmensuer, Emre Akbas, and Ahmet Acar, “Colorectal cancer tumor grade segmentation: A new dataset and baseline results,” *Heliyon*, vol. 11, pp. e42467, 02 2025.
- [12] Tete Xiao, Yingcheng Liu, Bolei Zhou, Yuning Jiang, and Jian Sun, “Unified perceptual parsing for scene understanding,” in *Proceedings of the European conference on computer vision (ECCV)*, 2018, pp. 418–434.
- [13] Meng-Hao Guo, Cheng-Ze Lu, Zheng-Ning Liu, Ming-Ming Cheng, and Shi-Min Hu, “Visual attention network,” *Computational visual media*, vol. 9, no. 4, pp. 733–752, 2023.
- [14] Jonathan Long, Evan Shelhamer, and Trevor Darrell, “Fully convolutional networks for semantic segmentation,” in *Proceedings of the IEEE conference on computer vision and pattern recognition*, 2015, pp. 3431–3440.
- [15] René Ranftl, Katrin Lasinger, David Hafner, Konrad Schindler, and Vladlen Koltun, “Towards robust monocular depth estimation: Mixing datasets for zero-shot cross-dataset transfer,” *IEEE Transactions on Pattern Analysis and Machine Intelligence (TPAMI)*, 2020.
- [16] Zhengzhong Tu, Hossein Talebi, Han Zhang, Feng Yang, Peyman Milanfar, Alan Bovik, and Yinxiao Li, “MaxViT: Multi-axis vision transformer,” *ECCV*, 2022.
- [17] Ant Duru and Alptekin Temizel, “Adaptive augmentation policy optimization with LLM feedback,” *arXiv preprint arXiv:2410.13453*, 2024.
- [18] L Roszkowiak, A Korzynska, J Zak, Dorota Pijanowska, Z Swiderska-Chadaj, and Tomasz Markiewicz, “Survey: interpolation methods for whole slide image processing,” *Journal of microscopy*, vol. 265, no. 2, pp. 148–158, 2017.
- [19] Ting-Yu Liao, Ching-Hui Yang, Yu-Wen Lo, Kuan-Ying Lai, Po-Huai Shen, and Youn-Long Lin, “Hardnet-dfus: Enhancing backbone and decoder of hardnet-mseg for diabetic foot ulcer image segmentation,” in *Diabetic Foot Ulcers Grand Challenge*, pp. 21–30. Springer, 2022.
- [20] Ping Chao, Chao-Yang Kao, Yushan Ruan, Chien-Hsiang Huang, and Youn-Long Lin, “Hardnet: A low memory traffic network,” in *2019 IEEE/CVF International Conference on Computer Vision (ICCV)*, 2019, pp. 3551–3560.
- [21] Haotian Yan, Chuang Zhang, and Ming Wu, “Lawin transformer: Improving semantic segmentation transformer with multi-scale representations via large window attention,” *arXiv preprint arXiv:2201.01615*, 2022.
- [22] Jakob Nikolas Kather, Niels Halama, and Alexander Marx, “100,000 histological images of human colorectal cancer and healthy tissue,” Apr. 2018.
- [23] Andrey Ignatov and Grigory Malivenko, “Nct-crc-he: Not all histopathological datasets are equally useful,” in *European Conference on Computer Vision (ECCV 2024)*, 2024.
- [24] James Kirkpatrick, Razvan Pascanu, Neil Rabinowitz, Joel Veness, Guillaume Desjardins, Andrei A. Rusu, Kieran Milan, John Quan, Tiago Ramalho, Agnieszka Grabska-Barwinska, Demis Hassabis, Claudia Clopath, Dharshan Kumaran, and Raia Hadsell, “Overcoming catastrophic forgetting in neural networks,” *Proceedings of the National Academy of Sciences*, vol. 114, no. 13, pp. 3521–3526, 2017.
- [25] MMSegmentation Contributors, “MMSegmentation: Openmmlab semantic segmentation toolbox and benchmark,” <https://github.com/open-mmlab/mms Segmentation>, 2020.
- [26] Richard J Chen, Tong Ding, Ming Y Lu, Drew FK Williamson, Guillaume Jaume, Bowen Chen, Andrew Zhang, Daniel Shao, Andrew H Song, Muhammad Shaban, et al., “Towards a general-purpose foundation model for computational pathology,” *Nature Medicine*, 2024.
- [27] Zhe Chen, Yuchen Duan, Wenhai Wang, Junjun He, Tong Lu, Jifeng Dai, and Yu Qiao, “Vision transformer adapter for dense predictions,” *arXiv preprint arXiv:2205.08534*, 2022.